DOI: 10.1002/asia.200600408

Improving MCM-41 as a Nitrosamines Trap through a One-Pot Synthesis

Jia Hui Xu,[a] Ting Ting Zhuang,[a] Yi Cao,[a] Jing Yang,[a] Jing Jia Wen,[a] Zheng Ying Wu,[a] Chun Fang Zhou,[a] Li Huang,[a, b] Ying Wang,*[b] Ming Bo Yue,[a] and Jian Hua Zhu*[a]

Abstract: Copper oxide was incorporated into MCM-41 by a one-pot synthesis under acidic conditions to prepare a new mesoporous nitrosamines trap for protection of the environment. The resulting composites were characterized by XRD, N_2 adsorption–desorption, and H_2 temperature-programmed reduction techniques, and their adsorption capabilities were assessed in the gaseous adsorption of *N*-nitrosopyrrolidine (NPYR). The adsorption isotherms were consistent with the Freundlich equation. The copper salt was deposited onto MCM-41 during the evaporation stage and was fixed on the host in the calcination process that followed. MCM-41 was able to capture NPYR in air below 373 K but not at 453 K. Loading of copper oxide on MCM-41 greatly improved its adsorption capability at elevated temperatures. The influence of the incorporation of copper into MCM-41 samples and the adsorption behavior of these samples are discussed in detail.

Keywords: adsorption · environmental chemistry · mesoporous materials · nanostructures · synthetic methods

Introduction

The modification of mesoporous silica materials is crucial for their potential applications as adsorbents and catalysts,[1,2] especially in areas of environmental protection such as the removal of carcinogenic pollutants. The fight against cancer is one of the challenges scientists face in the life sciences, and the removal of carcinogenic compounds from the environment is an important step in this effort. One new developing area of study is the filtration of nitrosamines from tobacco smoke. The pollution caused by cigarette smoking is a global problem, because cigarette smoke and its condensates contain many mutagenic, carcinogenic, and cocarcinogenic substances, and tobacco smoking is associated with about 30% of cancer deaths in the United States[3] and with all cancers in males worldwide.[4] Among the various toxic compounds, nitrosamines are strongly carcinogenic; in smokers and passive smokers,[5] they cause not only cancers of the lung but also of the larynx, oral cavity and pharynx,[6] pancreas, kidney, and bladder. Furthermore, a positive association between cigarette smoke and risk of breast or liver cancer was also reported.[7,8] With the characteristic functional group N–NO in their structure, nitrosamines can result in serious health risks even in trace amounts.[9,10]

Nitrosamines are widespread in the environment, from industrial workplaces such as rubber factories to tobacco smoke in the air, so the control of nitrosamine pollution is of growing interest. However, it is difficult to remove these carcinogens selectively in smoke despite the great effort being made in the development of cigarette filters.[11–13] Tobacco smoke is an aerosol composed of volatile agents in the vapor phase and semi- and nonvolatile compounds in the particulate matter, all of which totals more than four thousand compounds.[14] To decrease the level of nitrosamines in such a complex chemical system would involve the knowledge of how to discriminate and to trap the targets among the thousands of components of cigarette smoke. Therefore, any progress in this field is important for the deeper understanding of selective adsorption.

Zeolite was first chosen to lower nitrosamine levels in cigarette smoke.[15–17] The cations of zeolite exhibit an affinity

[a] J. H. Xu, T. T. Zhuang, Dr. Y. Cao, J. Yang, J. J. Wen, Dr. Z. Y. Wu, Dr. C. F. Zhou, L. Huang, Dr. M. B. Yue, Prof. Dr. J. H. Zhu
Key Laboratory of Mesoscopic Chemistry of the MOE
School of Chemistry and Chemical Engineering
Nanjing University
Nanjing 210093 (China)
Fax: (86) 25-8331-7761
E-mail: jhzhu@netra.nju.edu.cn

[b] L. Huang, Prof. Dr. Y. Wang
Ecoenergy and Ecomaterials Center (EEMC)
Nanjing University
Nanjing 210093 (China)
Fax: (86) 25-8368-6632
E-mail: wangy@netra.nju.edu.cn

with the N–NO group of nitrosamines, which has a negative charge. The strong electrostatic interaction promotes the adsorption of nitrosamines by zeolite. However, there are many different nitrosamines in smoke, and their molecular volumes and volatilities are all dissimilar.[18] The narrow channels of zeolite limits the adsorption of nitrosamines with big molecular volumes. Consequently, mesoporous silica was chosen as an alternative adsorbent. Both MCM-41 and SBA-15 can overcome the size constraint of zeolite pores and allow the introduction of larger molecules through the pores. As expected, SBA-15 exhibited a higher activity in the catalytic degradation of tobacco-specific nitrosamines (TSNA) than zeolite, because its wide channels can accommodate bulky carcinogens.[19] Volatile nitrosamines, also found in cigarette smoke, cannot be efficiently adsorbed by mesoporous silica because of their small molecular sizes (<0.9 nm) and high volatilities. Owing to their inherent siliceous compositions, MCM-41 and SBA-15 suffer from a lack of metal cations that provide the electrostatic affinity towards nitrosamines. Rather, MCM-41 did not show any capability in the adsorption of volatile nitrosamines at 453 K.[20] Many different methods were attempted to prepare the mesoporous catalysts. These catalysts included active components to overcome the weakness of electrostatic affinity to nitrosamines. It was noticed that direct synthesis was a time-saving method for the preparation of mesoporous catalysts. Incorporation of ferric or rare-earth components in SBA-15 in situ was adopted through a one-pot synthesis.[21] The coating of SBA-15 and MCM-41 with copper oxide by using this "incorporation in situ" method resulted in the enhanced adsorption of volatile nitrosamines by the composites.[22–24] Furthermore, insertion of copper salts into the SBA-15 synthesized also improved the mesoporous silica as a trap for volatile nitrosamines.[25,26] How the added metal oxides became incorporated into the mesoporous silica is still a question. At which stage of the synthesis the copper salt is incorporated into MCM-41 is also unknown. Moreover, the average pore size of resulting samples is often slightly increased,[23,26] but the reason for this is not well-understood. To answer these questions, a series of copper-modified MCM-41 samples were prepared, and their textural properties along with their adsorptive capabilities were investigated. There are no micropores in the structure of MCM-41, so the influence of copper oxide on the mesopore structure and its impact on the adsorption of nitrosamines can be clearly examined.

There are many potential applications for the mesoporous composites, for example, as adsorbents in aeration systems needed to trap nitrosamines at ambient temperature.[27] Thus, the adsorption of copper-modified MCM-41 composites was studied at 338 K; two related porous materials, NaY zeolite and hydrotalcite, were also assessed for comparison with MCM-41. *N*-nitrosopyrrolidine (NPYR), a volatile nitrosamine with a five-membered ring, was selected as the target for adsorption. Lastly, the MCM-41 sample containing copper was added to the filters of cigarettes to assess its reduction of nitrosamines in cigarette smoke.

Abstract in Chinese:

原位合成的 CuO 改性 MCM-41 是清除挥发性亚硝胺的吸附新材料，可望应用于环境保护与烟草降害。新材料经 XRD、N_2 吸附-脱附、H_2 TPD 等方法进行表征，采用吡咯烷亚硝胺（NPYR）的气相吸附评价其吸附性能，发现吸附等温线符合 Freundlich 吸附方程。合成过程中蒸发母液时铜盐沉积在 MCM-41 表面，焙烧后紧密结合。MCM-41 在 373 K 高效吸附 NPYR，但在 453 K 则不能吸附。负载 CuO 使得 MCM-41 能在高温吸附亚硝胺，铜组分的分布状态及其亚硝胺吸附作用在文中被详细讨论。

Results

Impact of Copper Oxides on the Pore Structure of MCM-41

To identify the impact of the copper guest on the structure and function of MCM-41, the samples were prepared under acidic conditions in different ways. The sample M5 was synthesized in the normal way with 5 wt% CuO and then thoroughly washed; hence, almost no copper remained in the sample. The sample bM5 was evaporated with the synthetic mother liquor at 353 K and then thoroughly washed so that only a few guests persist in the composite. After calcination, bM5 was named aM5. The sample cM5 was also evaporated with the mother liquor at 353 K, but calcination followed; therefore, all the copper additives are loaded onto the porous material. Table 1 lists the inductively coupled plasma (ICP) spectrometric analysis data of M5 and aM5. About 70 ppm of the copper species survived in the sample of M5, whereas aM5 consisted of 280 ppm of copper. However, the copper content of the cM5 sample calculated from H_2 tem-

Table 1. Textural properties of MCM-41 coated with copper species by the one-step synthesis.[a]

Property	MCM-41	M5	cM1	cM3	cM5	aM5	cM10
S_{BET} [$m^2 g^{-1}$]	1122	1048	1252	1237	1080	1243	774
V_{total} [$cm^3 g^{-1}$]	0.583	0.519	0.833	0.897	0.701	0.798	0.486
D_p [nm]	2.1	2.1	2.49	2.56	2.54	2.45	2.59
a_0 [nm]	3.58	3.57	4.05	4.08	4.03	3.87	4.12
Wall thickness [nm]	1.48	1.47	1.56	1.52	1.49	1.42	1.53
CuO [wt%]	–	0.0068	1.01	3.55	5.54	0.028	9.45

[a] See Experimental Section for designations of compounds.

perature-programmed reduction (TPR) test results was around 5 wt%, which is hundred times higher than the other two. Comparison of the copper content of the three composites clearly shows that the copper species begin to adsorb and/or deposit onto MCM-41 in the evaporation stage of the one-pot synthesis, but most are fixed and stabilized on MCM-41 in the following calcination stage.

Figure 1 illustrates the low-angle XRD patterns of copper-modified MCM-41. All the samples show an intense diffraction (100) peak. However, additional (110) and (200)

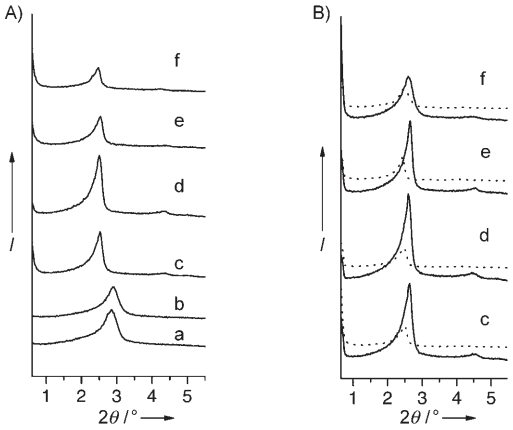

Figure 1. Low-angle XRD patterns of MCM-41 and the copper-modified samples. A) cM*n*; B) bM*n* (•••••) and aM*n* (——). a = MCM-41, b = M5, c = *i*M1, d = *i*M3, e = *i*M5, f = *i*M10.

peaks are unclear owing to the acidic synthesis conditions (Figure 1 A). The silica species always appear as less-condensed, linear oligomers under acidic conditions,[28] and the synthesis temperature of our experiment (303 K) is much lower than that of the samples synthesized in alkaline solution. Therefore, the MCM-41 synthesized under acidic conditions often exhibits indistinct (110) and (200) XRD peaks.[29,30] Incorporation of a certain amount of Cu doping in MCM-41 can stabilize the mesoporous structure, but overloading leads to the collapse of the mesopores. The cM1 and cM3 samples show stronger (100) peaks than the parent MCM-41, but the (100) peak intensity of the cM10 composite is slightly lowered. This means that there is a distortion of the long-range ordering of the mesoporous structure and/or the hexagonal array.[31,32] Furthermore, the loading of copper in MCM-41 caused the 2θ value of the (100) diffraction peak to decrease from 2.85 to around 2.50° (Table 1), whereas the corresponding cell parameter a_0 increased from 3.58 to 4.05–4.12 nm. This indicates that the composites have enlarged unit-cell dimensions.

Figure 1 A shows the XRD patterns of M5 and cM5 samples, and Table 1 depicts their textural properties. The existence of about 70 ppm copper species in M5 has little influence on the resulting structure: the 2θ value of its (100) peak (2.86°) and a_0 (3.57 nm) are almost the same as those of MCM-41. The corresponding values of the bM5 sample are 2.50° and 4.08 nm. After calcination, they increased to 2.62° and 3.89 nm (Figure 1 B), owing to structure shrinkage during calcination.[33] As seen in Figure 1 B, this shift in the (100) peak was also observed in the XRD patterns of other aM*n* and bM*n* samples. When the data for pore volume (V_{total}), pore diameter (D_p), and wall thickness shown in Table 1 are compared, it is likely that the structure of M5 is similar to that of MCM-41, and the structure of aM5 is close to that of cM5. Undoubtedly, the difference in copper content causes the different pore structures in the samples of M5 and aM5. Velu et al. reported the impact of copper species on the structure of MCM-41 samples, and they found that the ordering of MCM-41 deteriorated when the copper content was increased to 4.2 wt%.[32] Similarly, our results imply that the detectable structural differences in copper-containing MCM-41 are caused at a much lower copper content in the one-pot synthesis.

Figure 2 A shows the nitrogen-adsorption isotherms of the MCM-41 samples, and Table 1 lists the parameters derived from them. All the isotherms are type IV, which is characteristic of mesoporous solids. The data show a well-defined step between the P/P_0 range of 0.15–0.3 in the isotherms, owing to the capillary condensation of N_2 molecules in the uniform mesopores of MCM-41. Copper modification enlarges the surface area and pore volume of the cM1 and

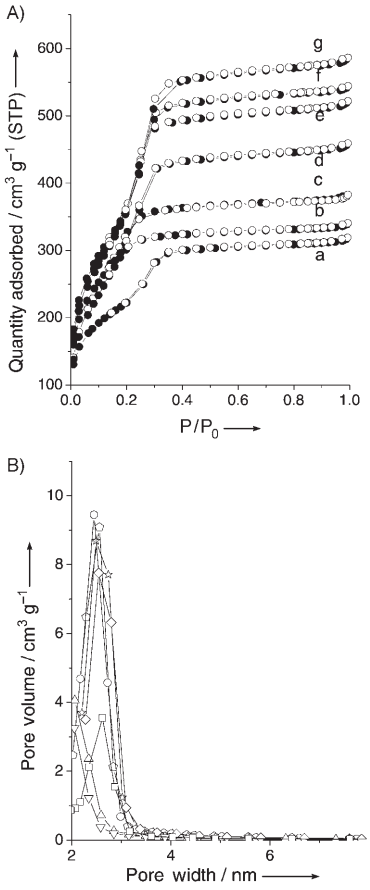

Figure 2. A) N_2 adsorption–desorption isotherms (○ = adsorption, ● = desorption) and B) pore-size distribution of cM10 (a, □), M5 (b, ▽), MCM-41 (c, △), cM5 (d, ◇), aM5 (e, ○), cM1 (f, ☆), and cM3 (g, ⬠).

CHEMISTRY
AN ASIAN JOURNAL

cM3 samples. For cM5, its pore volume is larger than that of MCM-41, but its surface area is similar. A 10 wt% loading of copper oxide on MCM-41 caused the specific surface area and pore volume to decrease significantly (Table 1). MCM-41 has a pore size of 2.1 nm due to the acidic synthesis conditions; this value coincides with those in the literature.[29,34,35] On the other hand, all the cM*n* samples have larger average pore sizes of 2.5–2.6 nm (Figure 2B). The most-significant change was displayed by cM10, whose pore size increased from 2.1 to 2.59 nm. Clearly, the hydrothermal treatment in the mother liquor resulted in pore expansion.[30] Similar phenomena were observed in SBA-15 modified with copper oxide or magnesia with the one-pot synthesis[23,36] and were attributed to the salt effect. The addition of salts in the synthesis system leads to the formation of helical crown ether like metal–PEO (poly(ethylene oxide)) complexes, which are not strong enough to incorporate M^{n+} cations into the SBA-15 mesostructure. However, M^{n+} cations still exert some impact on templating and silicate hydrolysis.[37,38] The specific surface area, pore volume, and pore size of aM5 are larger than those of MCM-41, which is consistent with the results of low-angle XRD. In contrast, M5 exhibited the same textural parameters as those of MCM-41 below experimental error. It appears that the copper salt in the channel of MCM-41 alters the pore structure, and the evaporation stage in the one-pot synthesis enables the copper species to be deposited on the surface of the composite and hence enlarge the pore size. In the initial stage of the hydrothermal synthesis, the copper species may interact preferably with water molecules and not with the silica species. As water evaporates from the mother liquor, copper–water complexes become copper–surfactant compounds. Thus, the copper species have a strong interaction with the silica walls. As the interaction of the guest with the MCM-41 surface is expected to consume silanol groups, careful analysis of the IR transmission spectra of MCM-41 and the copper-modified samples was carried out. The stretching modes of the surface silanol groups (≡Si–OH) give rise to the band at 960 cm^{-1} for most ordered mesoporous materials, thus indicating the presence of perturbed or defect groups. This band appeared near 960 cm^{-1} in MCM-41 but with lower intensity in cM5 (Figure 3), which means that some surface silanol groups are consumed in the one-pot synthetic process. The copper species coated in MCM-41 probably prevent pore shrinkage in the following calcination stage.[33]

High-angle XRD and H_2 TPR were used to check the distribution and state of the copper species in MCM-41. Crystalline CuO was found in all the cM*n* samples, but the crystalline Cu_2O phase only emerged when the coating amount exceeded 3 wt% (Figure 4A). A similar situation was previously reported: in the CuO/SBA-15 samples that were prepared in the one-pot synthesis, crystalline CuO appeared in the sample with 3% CuO/SBA-15.[22] The distribution of copper guest in the host seems complex: as the host surface has varying degrees of curvature, the copper species is not deposited uniformly throughout, such as on planar substrates or core–shell particles.[39] The unevenness of deposition, however, depends on the morphology of the hosts. The hosts form a heterorganic distribution in which the guest is aggregated to form XRD-visible particles, but some guests cannot even form a monolayer.[24] These phenomena conflict with the high dispersion of copper oxide on SBA-15 or MCM-41 with the solvent-free method,[23,26] which is probably related to the existence of the template and the evaporation stage in the one-pot synthesis. However, the reason for this is still undetermined. Figure 4B displays the TPR profiles of copper-modified MCM-41 according to normalized H_2 consumption. No reduction was found in the samples of MCM-41, M5, and aM5 from 303 to 873 K. A strong peak centered at around 467 K with a smaller peak at 503 K emerged for the cM*n* samples. The peak intensities increased as the amount of copper was raised. Another small peak appeared at around 750 K, but its intensity did not change between samples. For cM5, another peak appeared near 720 K, and its height increased for cM10. According to the literature,[40,41] the peak at around 470 K in the cM*n* samples corresponds to reduction of the copper–oxygen phase,[38] and the peaks at around 720 and 750 K result from reduction of the crystalline Cu_2O and/or copper silicate.[41] Hydrogen consumption at 503 K is associated with reduction of finely dispersed copper oxide to copper metal inside the

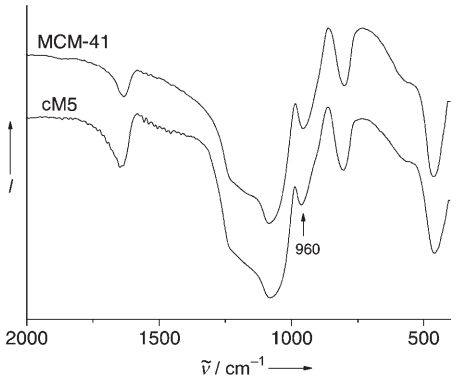

Figure 3. FTIR spectra of MCM-41 and CM5.

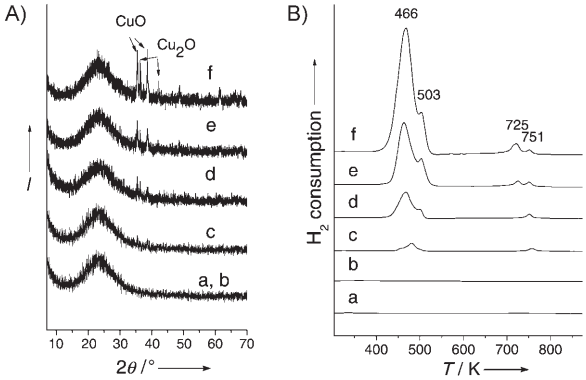

Figure 4. A) High-angle XRD patterns and B) H_2 TPR spectra of copper-modified MCM-41 samples. a = MCM-41, b = M5, c = cM1, d = cM3, e = cM5, f = cM10.

channel of mesoporous silica,[26,40] and the constant T_{max} reflects the invariability in CuO particle size. The amount of H_2 consumed in the TPR process, as calculated from the sum of the reduction peaks, is close to the amount of copper added in the synthetic solution of the sample of cM5 (Table 1).

Promotion of Adsorption of Volatile Nitrosamines in MCM-41 by Copper Oxide

Figure 5A shows the adsorption of NPYR by MCM-41 at 338 K. NPYR is a volatile nitrosamine with a molecular diameter of 0.42×0.54 nm, so it easily enters and diffuses

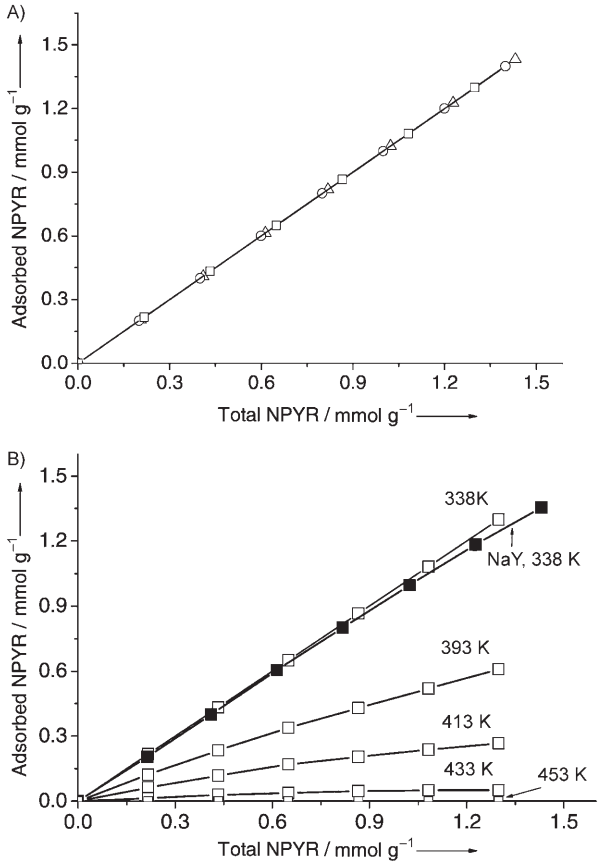

Figure 5. Impact of A) rate of carrier gas (338 K; △ = 10, ○ = 20, □ = 30 mL min^{-1}) and B) temperature on the adsorption of NPYR on MCM-41.

inside the channel of MCM-41. In the instantaneous adsorption, the rate of flow of carrier gas changed from 10 to 30 mL min^{-1}, and 100% of NPYR was captured by MCM-41 at 338 K (Figure 5A). The volume of MCM-41 adsorbent was about 0.038 mL, so when the rate of flow of carrier gas reached 10 mL min^{-1}, the contact time of NPYR with the whole adsorption bed was 0.23 s. When the rate of flow of carrier gas increased to 30 mL min^{-1}, the contact time decreased to 0.08 s. This means that the variation in adsorbent–adsorbate contact time from 0.23 to 0.08 s does not affect the mass-transfer characteristics of the adsorbate in the adsorbent. Furthermore, MCM-41 exhibited a high ability to trap nitrosamines in gas flow in the temperature range 338–373 K owing to its large pore volume, whereas the zeolite NaY showed an inferior capability at 338 K (Figure 5B). As the accumulated amount of NPYR reached 1.5 mmol g^{-1}, NaY was able to adsorb about 90% of the NPYR. When the accumulated amount reached 2.0 mmol g^{-1}, this proportion decreased to 83%. This is the first observation that mesoporous silica is superior to zeolite in the adsorption of volatile nitrosamines at ambient temperatures.

However, the adsorptive capability of MCM-41 dramatically declined as the temperature rose over 373 K (Figure 5B), until finally it could not adsorb anymore NPYR when the temperature reached 453 K. Owing to a lack of strong adsorption sites, the nitrosamines could not be held by the mesoporous adsorbent.[26] In contrast, NaY still adsorbed 73% of the NPYR in the gas flow at 453 K. MCM-41 is not the only mesoporous silica to lose the ability to trap NPYR at elevated temperatures. As illustrated in Figure 6A, SBA-15 adsorbed 97% of NPYR at 373 K, but its adsorptive capability also declined as the temperature rose. Owing to the existence of micropores in its structure,[42] SBA-15 still captured 5% of NPYR in the gas stream at 453 K.

Figure 6A shows the influence of incorporating copper in MCM-41 on the adsorption of NPYR at elevated temperatures. The M5 sample consists of 68 ppm copper, but its adsorptive ability fell significantly as the temperature increased, just as with the parent MCM-41. Finally, M5 failed to trap NPYR in the stream at 453 K. Different situations were observed for the cM5 sample. Incorporation of copper oxides increased the pore size of the sample from less than 2.0 to 2.5 nm (Table 1), which should be disadvantageous for providing the necessary geometric confinement for tiny adsorbates such as volatile nitrosamines. As with MCM-41 and M5, the cM5 sample adsorbed all the NPYR in the stream at 338 K. As the temperature rose from 393 to 433 K, cM5 exhibited a significantly larger capacity than MCM-41 or M5 in the adsorption of NPYR under the same conditions. When the temperature increased to 453 K, both MCM-41 and M5 were inactive in the adsorption of NPYR, but cM5 could trap about 25% of the nitrosamines in the gas stream.

For an overall analysis of the adsorption isotherms, we correlated the experimental equilibrium data with the Freundlich equation in its linear form, that is, $\ln q = \ln K_F + 1/n \cdot \ln C$, in which q is the amount of nitrosamines adsorbed per gram of adsorbent, C is the total amount of nitrosamines passed through each gram of zeolites, K_F is the known Freundlich constant related to adsorbent capacity, and $1/n$ is the factor related to adsorption strength as well as favorability.[37,43] Table 2 lists the isotherm parameters calculated with the method of least squares, which reveals the influence of temperature and the incorporation of copper in MCM-41 on the adsorption of volatile nitrosamines in the gas stream.

Figure 6B shows the adsorption of NPYR by copper-containing MCM-41 samples at 453 K. On the basis of the last

CHEMISTRY
AN ASIAN JOURNAL

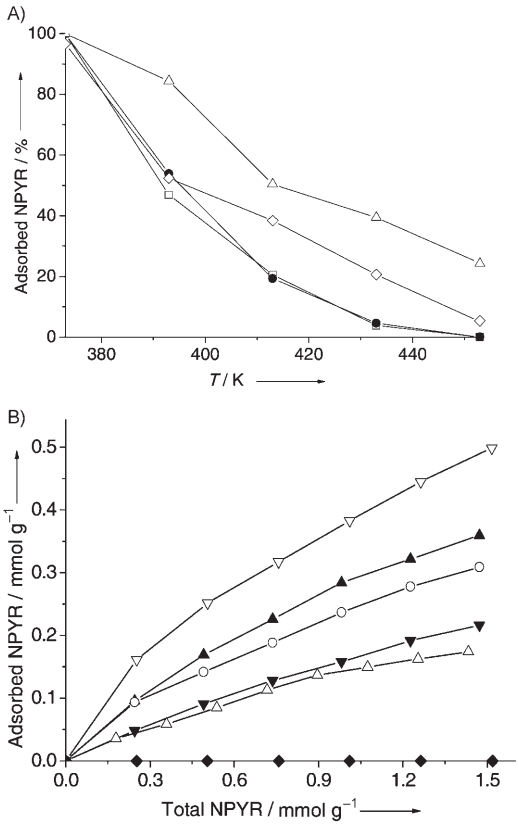

Figure 6. A) Adsorption of NPYR by MCM-41 and copper-modified samples at different temperatures: □ = MCM-41, ● = M5, △ = cM5, ◇ = SBA-15. B) Variation in amount of adsorbed NPYR versus total amount for the copper-modified samples at 453 K: ▽ = cM10, ▲ = cM5, ○ = cM3, ▼ = cM1, △ = aM5, ◆ = M5.

Table 2. Freundlich constants of the adsorption isotherms of NPYR in mesoporous silica.[a]

Adsorbent	T [K]	K_F	n	R^2
MCM-41	338	1	1	1
	393	0.4879	1.120	0.9993
	413	0.2260	1.235	0.9936
	433	0.0480	1.327	0.9516
M5	373	1	1	1
cM5	393	0.5517	1.069	1
SBA-15	413	0.2096	1.243	0.9997
aM5	433	0.0539	2.696	0.8366
cM1	373	1	1	1
cM3	393	0.9028	1.106	0.9975
cM10	413	0.5375	1.256	0.9992
	433	0.4347	1.412	0.9996
	453	0.2793	1.345	0.9966
	373	0.9824	1.017	0.9999
	393	0.5679	1.248	0.9999
	413	0.4139	1.145	0.9991
	433	0.2323	1.235	0.9990
	453	0.056	1.462	0.9922
	453	0.1390	1.266	0.9930
	453	0.1609	1.194	0.9982
	453	0.2372	1.472	0.9974
	453	0.3826	1.488	0.9996
NaY	338	0.9982	1.002	1
1% CuO/NaY[b]	453	0.9232	1.084	0.9975
3% CuO/NaY[b]	338	0.9465	1.060	0.9993
Hydrotalcite (HT)	453	0.9648	1.035	0.9995
10% CuO/HT[b]	338	0.9892	1.014	0.9996
	453	0.9765	1.030	0.9988
	338	0.1744	2.071	0.9953
	453	0.0746	1.993	0.9599
	338	0.5444	1.354	0.9971
	453	0.4895	1.260	0.9979

[a] Conditions: 338–453 K, NPYR in dichloromethane, flow rate of carrier gas 30 mL min^{-1}. [b] See Experimental Section for the designations of compounds.

data point on the isotherms, it is clear that incorporation of copper oxide in MCM-41 enhances the adsorption capability at 453 K, and the more copper that is loaded, the more NPYR is adsorbed. As the accumulated amount of NPYR passing through the adsorbent reached 1.2 mmol g^{-1}, M5 became incapable of adsorption, whereas aM5 captured 0.16 mmol g^{-1}, which was slightly less than for cM1 (0.19 mmol g^{-1}). Under the same conditions, cM3 and cM5 adsorbed 0.27 and 0.32 mmol g^{-1}, respectively, whereas about 0.43 mmol g^{-1} of NPYR was trapped by the sample of cM10. Similar relationships between the loading amount of copper in MCM-41 and the adsorbed amount of NPYR were also observed in gaseous adsorption with a different quantity of NPYR (Figure 7A), a finding supported by the variation of K_F shown in Table 2. As the loading amount of copper oxide in MCM-41 increased from 1 to 10 wt%, the corresponding value of K_F gently rose. Closer inspection revealed that aM5 is highly efficient in the adsorption of NPYR, especially during the initial period when the accumulated amount of NPYR is small. For example, aM5 exhibited the same adsorption capability as cM1 when the amount of NPYR passing through the adsorbent reached 0.2 mmol g^{-1}, although cM1 contains 30 times more copper than aM5. However, as the accumulated quantity of NPYR increased, the advantage of aM5 gradually faded away. To capture a large quantity of NPYR in the gas stream, it is necessary for MCM-41 to have a high copper content (Figures 6B and 7A). With 10 wt% copper loaded, cM10 adsorbed about 33% of the NPYR in the stream at 453 K. The N–NO groups of volatile nitrosamines are strongly attracted to the copper cations in the adsorbent;[26] therefore, the adsorption of NPYR on cM*n* is stronger than MCM-41 at 453 K, and, consequently, the following experiments were performed on samples of cM*n*.

Figure 7B shows the adsorption of NPYR on arenaceous quartz and amorphous silica before and after loading of copper oxide. Only a little NPYR was trapped by arenaceous quartz at 338 K, and loading of copper oxide did not enhance the adsorption of volatile nitrosamines. In fact, the adsorption decreased slightly in the resulting composite. A similar situation was observed in amorphous silica. As shown in Figure 7B, amorphous silica exhibits a considerable ability to adsorb NPYR at 338 K. When the accumulated amount of NPYR reached 1.0 mmol g^{-1}, about 89% of the adsorbate was captured. However, loading of copper oxide (10 wt%) on the silica lowered this value to 78%. Notably, copper oxide itself hardly adsorbed NPYR, and only 4% of

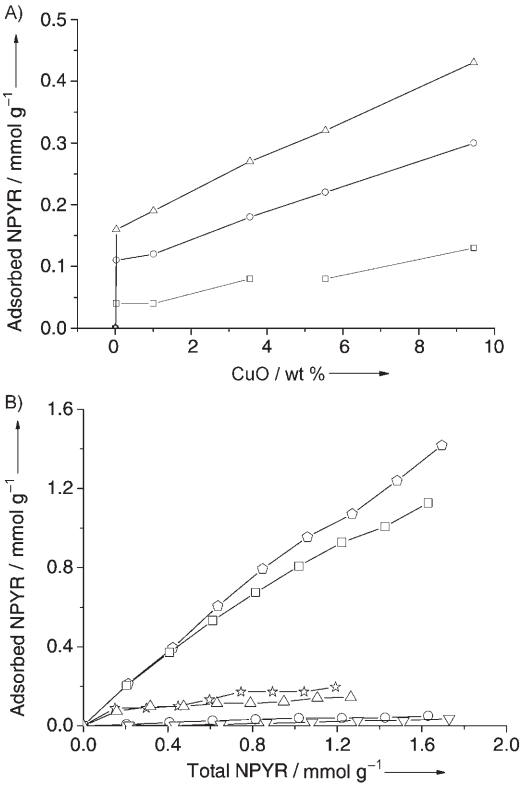

Figure 7. Effect of loading of copper oxide in A) MCM-41 at 453 K ($\triangle$ = 1.2, $\bigcirc$ = 0.7, $\square$ = 0.2 mmol g^{-1} accumulated NPYR in the gas stream) and B) quartz and amorphous silica at 338 K ($\pentagon$ = SiO_2, $\square$ = 10% CuO/SiO_2, $\star$ = 10% CuO/SiO_2, 453 K, $\times$10, $\triangle$ = SiO_2, 453 K, $\times$10, $\bigcirc$ = 10% CuO/quartz, $\triangledown$ = quartz) on the adsorption of NPYR.

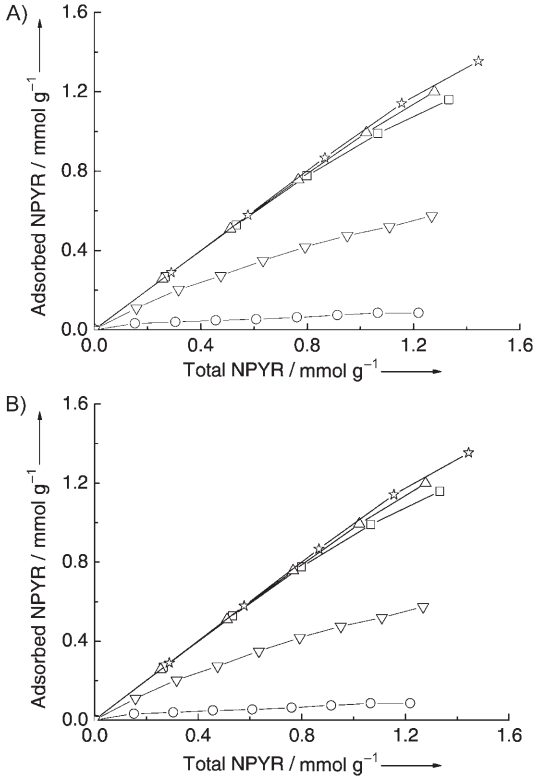

Figure 8. Influence of copper modification on the adsorption of NPYR on zeolite NaY and hydrotalcite at A) 338 K and B) 453 K. $\square$ = NaY, $\triangle$ = 1% CuO/NaY, $\star$ = 3% CuO/NaY, $\triangledown$ = 10% CuO/HT, $\bigcirc$ = HT.

nitrosamines were adsorbed when about 1.0 mmol g^{-1} of NPYR was passed through the oxide (not shown). This adsorption amount is much less than that of silica; there was thus no improvement but, rather, a decrease in adsorption of NPYR in the sample containing 10 wt% copper oxide at 338 K. When the temperature was increased to 453 K, the adsorption ability of silica declined significantly, and only 1% of NPYR was trapped when 1.0 mmol g^{-1} of adsorbate was passed through the adsorbent. In contrast, the 10% CuO/SiO_2 sample showed a slightly higher adsorption capability, and about 2% of the NPYR in the gas stream was captured (Figure 7B).

Figure 8 shows the adsorption of NPYR on zeolite NaY and hydrotalcite (HT) before and after copper modification at different temperatures. As mentioned above, NaY has an adsorption capacity inferior to that of MCM-41 at 338 K (Figure 5B), probably due to the smaller surface area (766 m^2 g^{-1}) and pore volume (0.31 cm^3 g^{-1}). Loading of 1 wt% CuO on NaY failed to enhance but slightly lowered its adsorption ability, and incorporation of 3 wt% CuO in the zeolite did not elevate the adsorption capacity of NaY either. On the contrary, hydrotalcite exhibited a weak ability to capture NPYR at 338 K because of its small surface area (245 m^2 g^{-1}), and CuO loading dramatically improved the adsorption. As the temperature was increased to 453 K, less NPYR was trapped by NaY, although modification with copper promoted the adsorption. Both copper-modified samples showed a larger K_F value than the parent zeolite, thus mirroring the improved adsorption capability (Table 2). When about 1.2 mmol g^{-1} of NPYR was passed through the adsorbent, NaY trapped 90%, whereas 1% CuO/NaY and 3% CuO/NaY adsorbed 95% and 98%, respectively (Figure 8B). Increasing the temperature from 338 to 453 K also lowered the adsorption capacity of hydrotalcite and the copper-modified derivative. As the accumulated amount of NPYR reached 1.2 mmol g^{-1}, the adsorption capacity of HT decreased from 0.19 to 0.07 mmol g^{-1}, and that for 10% CuO/HT declined from 0.65 to 0.54 mmol g^{-1}. Consequently, the effect of copper on promoting the adsorption of NPYR in hydrotalcite became clearer at 453 K (Table 2).

Figure 9 shows the use of copper-containing MCM-41 in decreasing the nitrosamine levels of cigarette smoke. There is a considerable amount of nitrosamines in mainstream smoke (1.72 nmol per cigarette), and adsorption by mesoporous additives in filters clearly lowers the nitrosamine content. As a noncation adsorbent, MCM-41 trapped 12% of the carcinogenic agents in mainstream smoke at ambient temperatures. Compared with the results of MCM-41 in the adsorption of NPYR at 338 K (Figure 5A), the proportion of nitrosamines removed in smoke is evidently lower due to the complex composition of tobacco smoke, with hundreds

CHEMISTRY
AN ASIAN JOURNAL

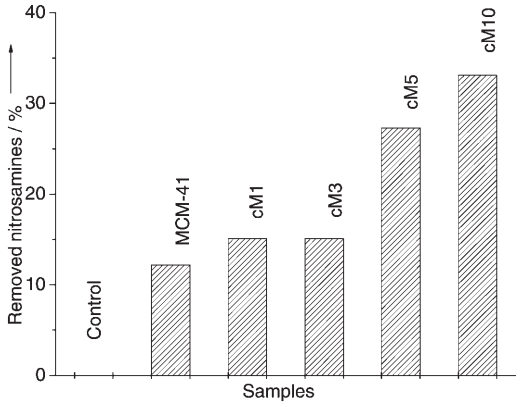

Figure 9. Removal of nitrosamines from mainstream cigarette smoke by addition of copper-modified samples in the cigarette filters.

of compounds competitively occupying the adsorption sites in MCM-41, thus hindering the adsorption of nitrosamines. Incorporation of small amounts of copper oxide in MCM-41 slightly enhanced the adsorption capability of the resulting composites, and about 15% of the nitrosamines were eliminated by the cM1 and cM3 samples (Figure 8). Increasing the amount of CuO guest to 5 wt% enabled MCM-41 to adsorb 27% of the nitrosamines in smoke, whereas cM10 can remove 33% of the harmful constituents. On the other hand, NaY zeolite showed good adsorption ability by trapping 27% of the nitrosamines in smoke, a similar result to that for cM5 but inferior to cM10.

Discussion

A comparison of M5, aM5, and cM5 samples can provide clues as to how the copper is incorporated into MCM-41 in the one-pot synthesis and how the guest affects the property–function relation of the host. The same amount of copper salt was added to the mother liquor to synthesize the above samples, but the resulting composites have significantly different amounts of copper depending on the treatment they received. The synthetic procedure of the M5 sample was the same as that of the parent MCM-41, in which the precipitate underwent filtering and washing. Thus, only a trace amount of copper remained in the sample. It is possible that almost all the copper is wrapped in the framework of MCM-41 instead of being located on the surface of the channel;[44] water would otherwise remove these copper species during washing. In our previous work,[23] a similar experiment was performed on a sample of 20% MgO/SBA-15 that was fully washed, dried, and calcinated, and the X-ray photoelectron spectroscopy (XPS) data clearly showed that this sample was free of magnesium. One confirmation of the postulate for copper comes from the characterization of the M5 sample, in which its textural property is similar to that of the parent MCM-41 (Table 1); this coincides with the report by Hartmann et al.[45] In other words, the remaining copper species do not prevent the shrinkage of the pores of MCM-41. This is different from the report on silica modified with 5 wt% copper oxide.[24] One may argue that the tiny amount of copper in M5 causes this difference. However, this argument is not justified by the sensitive assessment of the impact of copper measured by the adsorption of NPYR. The existence of copper in the M5 sample did not improve the adsorption of the volatile nitrosamines, thus indicating the isolation of these copper species inside the pore wall. Otherwise, the promotion of the adsorption of NPYR should be detectable because of the improved adsorption capacity of aM5 with a copper content only two times larger than that of the M5 sample. When the structural properties and adsorption behavior of M5, which are almost the same as MCM-41, are combined, it is very likely that most of the copper species are wrapped in the pore wall, and they do not show any obvious influence on the adsorption of volatile nitrosamines, especially at temperatures higher than 393 K (Table 2 and Figure 6A).

The textural property and adsorption capability of NPYR of aM5 is different from M5 but similar to cM1 (Table 1 and Figure 5B), although aM5 has a copper content (280 ppm) fairly close to that of M5 (68 ppm) but very different from that of cM1 (1.01 wt%). This distinct difference between M5 and aM5 cannot simply be attributed to the content of copper, but originates from the hydrothermal treatment in the synthesis. The sample aM5 was evaporated with the mother liquor before the washing stage, in which the metal species are able to interact with the silanol groups during the evaporation of water.[23] Apart from the copper anchored in the composite, the acidic route and the salt effect enables the versatile morphology to form;[29] thus, relatively small holes, kinks, and vacancies appear on the surface of the host, which result in the heterogeneous distribution of copper modifiers. In the following washing stage, only those copper species located and/or anchored on these defects can resist the purge of water and remain in the sample because the negative curvature of these defects slows the flush of water. A similar principle can be used to explain the high efficiency of aM5 in the adsorption of NPYR. When the NPYR molecules move to these defects, the specific curvature of the defect slows the flow of the carrier gas passing through, so the volatile nitrosamine molecules in the gas stream can be attracted and captured by the copper species located in the defect. The defects and/or intrawall micropores play a major role in controlling diffusion at low adsorbate concentration.[46–48] As a result, aM5 exhibits an adsorption ability comparable to that of cM1 in the initial adsorption (Figure 7A). Another piece of evidence that confirms the impact of geometric microenvironment on the function of copper modifiers is seen in Figure 7B, in which the same amount of CuO in quartz or amorphous silica to that in cM10 did not promote the adsorption of NPYR to a similar extent. Aggregation of copper oxide in silica may partly account for this difference.[49] The morphology or curvature of the channel affects the adsorption behavior of mesoporous silica as reported in the literature,[47,50,51] whereas a suitable geometric microenvironment is crucial for copper modifiers

to exert their influence. Furthermore, copper species can form a synergistic relationship with an adjacent silanol group in the adsorption of nitrosamines, as we previously reported,[26] and the curvature of the surface affects the bonding of the surface silanol groups.[30] The contribution of the silanol groups can be seen in the following discussion: As shown in Figure 6B, aM5 adsorbed about 0.17 mmol g^{-1} of NPYR at 453 K when its total amount reached 1.5 mmol g^{-1}. However, with the assumption that all the copper species are highly dispersed and thus in full contact with the NPYR molecules, the concentration of copper species assumed to be in the form of CuO is only 3.5 μmol g^{-1} in aM5. It is impossible for these copper sites to capture 10 times more NPYR adsorbates due to the limitation of space. Consequently, there must be a contribution from the surface silanol groups towards the adsorption. At first glance, this inference seems to conflict with the fact that neither MCM-41 nor M5 is active for adsorption at 453 K because they also have plenty of surface silanol groups. In our opinion, this variation results from the influence of two factors. The first is the existence of copper in aM5, which results in synergy with the silanol group, and the second is the structural defects inside the channel during evaporation as mentioned above. In general, the salt effect in hydrothermal treatment is attributed to the branching of micelles that causes the transition from hexagonal mesophase to disordered network.[30] The average pore size of aM5 is larger than that of the parent MCM-41 (Table 1), thus showing the existence of interaggregate pores.[52] Although these defects cannot be accurately distinguished by the standard Barret–Joyner–Halenda (BJH) method, their existence can be revealed through the adsorption of probe molecules such as volatile nitrosamines. Although cM1 has a copper content 30 times larger than aM5, the latter exhibits an adsorption capability towards NPYR at 453 K that is superior to M5 or MCM-41 but similar to cM1 when the amount of NPYR is under 0.3 mmol g^{-1}. The high efficiency of the aM5 composite in the adsorption of volatile nitrosamines provides information for the preparation of mesoporous-silica adsorbents with a higher efficiency for environmental protection: apart from the favorable pore structure, the new candidate should possess a suitable curvature or defects in the channels to accommodate the incorporated active components.

Unlike M5 and aM5, cM5 was not washed but was evaporated in the synthesis stage. Therefore, all the copper guests were deposited on its surface, a situation similar to that reported in which the copper species was grafted or anchored onto MCM-41.[53] Through a comparison with aM5, the impact of copper oxide deposition on the textural property of MCM-41 can be tentatively seen. Loading of more than 5.52 wt% CuO caused cM5 to lose 12% of its pore volume and 13% of its surface area, thus expanding the average pore size while thickening the pore wall (Table 1). At the same time, the corresponding surface concentration of copper rose to 0.693 mmol g^{-1}, 190 times more than that of aM5. However, these copper species do not bring significant benefits for cM5 in capturing NPYR (Figure 6B). In cases in which the amount of NPYR reached 0.2 mmol g^{-1}, cM5 trapped 0.079 mmol g^{-1}, whereas aM5 adsorbed 0.040 mmol g^{-1}. When the concentration of NPYR exceeded 1.2 mmol g^{-1}, the adsorption capacity of cM5 was still about double that of aM5. These results reflect the importance of the dispersion of copper in MCM-41 with regard to the adsorption of volatile nitrosamines. For the removal of trace nitrosamines in the gas stream of the aerator, it is possible to use MCM-41 modified with a spot of copper provided the promoter is highly dispersed. Apart from the larger loading of copper, the dispersion of copper species on cM5 is different from that of M5 or aM5. Both crystalline Cu_2O and CuO were detected in the XRD patterns of cM5 (Figure 4A); this indicates aggregation of the guest, which leads to a decreased efficiency of the copper modifier in improving the adsorption of NPYR. The aggregation of copper species in MCM-41 also makes the exploration of host–guest interactions difficult; for example, the consumption of surface silanol groups is not proportional with the absolute amount of copper species loaded on MCM-41 because the majority of guests is not well-dispersed and hence does not interact with the silanol groups.[54] On the basis of the results of XRD and FTIR, it is clear that part of the incorporated copper species is located inside the channels of MCM-41 and interacts with the surface silanol groups to change the unit-cell parameters and average pore size of the mesoporous silica, whereas the rest aggregates mainly on the external surface of the host to form the crystalline copper oxides detected by XRD.

A different situation is observed in the adsorption of mainstream cigarette smoke, for which numerous components other than nitrosamines competitively occupy the adsorption sites and the amount of nitrosamines reduced by copper-containing MCM-41 is proportional to its copper content. To remove nitrosamines from such a complex system, incorporation of copper into mesoporous siliceous materials such as MCM-41 through a one-pot synthesis to construct enough adsorption sites seems feasible and efficient.

Conclusions

Copper can be incorporated in situ in the mesoporous silica MCM-41 through a one-pot synthesis. Copper species begin to deposit onto MCM-41 at the evaporation stage and are fixed on the porous host at the following calcination stage, thus enlarging the average pore size of resulting composites. MCM-41 exhibits significant adsorption capacity for NPYR as long as the temperature stays below 373 K, but fails to trap the volatile nitrosamines at 453 K. Through the one-pot synthesis, copper cations in MCM-41 promote the adsorption of NPYR at elevated temperatures. Their NPYR adsorption isotherms are consistent with the Freundlich equation.

Experimental Section

NPYR was purchased from Sigma and dissolved in dichloromethane (analytical grade) at a ratio of 1:19 (*v*/*v*). Qingdao Haiyang (China) provided the chromatographic silica gel (100–200 mesh) with a surface area of 410 $m^2 g^{-1}$; the arenaceous quartz of 20–40 mesh used in the experiment was commercial quartz sand. Zeolite NaY, a commercially available powder with an Si/Al ratio of 2.86, a pore volume of 0.31 $cm^3 g^{-1}$, and a surface area of 766 $m^2 g^{-1}$, was stirred in aqueous NaCl (1 M, 10 mL g^{-1} zeolite) six times, washed till chloride-free, and calcinated in air prior to use. Copper was incorporated into the zeolite by using "drying impregnation": $Cu(NO_3)_2 \cdot 3H_2O$ (0.456 g) was dissolved in H_2O (40 mL), and NaY (5 g) was added. The mixture was stirred strongly, heated to half-dryness, and then dried at 373 K overnight. The product was ground to 100 mesh and calcinated at 773 K for 6 h to convert $Cu(NO_3)_2$ into copper oxide. The resulting sample contained 3% (*w*/*w*) CuO and is denoted 3% CuO/NaY. Other samples were prepared in the same way, and the concentration of the aqueous solutions was controlled to obtain different loading of copper cations. Hydrotalcite, with an Mg/Al ratio of 2, a surface area of 245 $m^2 g^{-1}$, and a pore volume of 0.75 $cm^3 g^{-1}$, was prepared according to literature procedures.[55] To prepare copper-modified hydrotalcite, $Cu(NO_3)_2 \cdot 3H_2O$ (0.304 g) was dissolved in H_2O (20 mL), and calcinated hydrotalcite (0.9 g) was added. The mixture was stirred at 303 K for 6 h, evaporated at 353 K, and then dried at 373 K overnight. The product was calcinated at 773 K for 6 h to afford the sample named 10% CuO/HT. Tetraethylorthosilicate (TEOS) and cetyltrimethylammonium bromide (CTAB) were from Shanghai Wulian and Lingfeng Companies (China), and other regents of analytical grade were used as received. Virginia-type cigarettes with a tar value of 15 mg per cigarette and a nicotine value of 1.2 mg per cigarette were purchased from the market.

MCM-41 was synthesized according to the literature.[34] To examine the impact of cupric salts in the synthetic solution of MCM-41, one sample was prepared with the same procedure as for MCM-41, the only exception being the addition of an amount of copper nitrate equivalent to 5 wt% CuO to the synthetic solution. After the filtering, washing, drying, and calcination stages, the sample obtained was denoted M5. To prepare copper-modified MCM-41 by the one-pot synthesis, CTAB (1.49 g) and the required amount of copper nitrate were dissolved in water (51.80 g), followed by the addition of hydrochloric acid (36%, 8.17 g). Finally, TEOS (4.25 g) was introduced with stirring at 303 K. The molar composition of the mixture was 5TEOS:1CTAB:xCu$(NO_3)_2 \cdot 3H_2O$:20HCl:764H_2O, in which x represents the loading level of CuO. After being stirred for 48 h, the mother liquor was evaporated with stirring at 353 K, and precipitates appeared. The resulting solid was divided into three parts. The first part was directly calcinated in air at 823 K for 6 h to obtain the composite denoted cM*n*, in which *n* represents the mass percentage of CuO in the sample. The second and third parts were thoroughly washed with distilled water until they became white. The second part was then air-dried and named bM*n*, in which *n* indicates the amount of copper (equivalent to CuO) added to the synthetic solution. After being air-dried, the third part was calcinated at 823 K in air for 6 h, and the sample obtained was denoted aM*n*.

XRD patterns of the samples were recorded on an ARL XTRA diffractometer with $Cu_{K\alpha}$ radiation in the 2θ range 0.5–8° or 5–70°. Nitrogen-adsorption and -desorption isotherms at 77 K were recorded on a Micromeritics ASAP 2020 system in which the sample was evacuated at 573 K for 4 h prior to testing. The Brunauer–Emmett–Teller (BET) specific surface area of the sample was calculated by using adsorption data in the relative pressure (P/P_0) range 0.04–0.2, and the pore volume was determined from the amount adsorbed at a relative pressure of about 0.99.

TPRs of the samples were carried out by using H_2/Ar (1:9 *v*/*v*) as reducing agent with a flow rate of 25 mL min^{-1}. A 0.1-g sample was placed in a quartz tube, treated with a flow of helium at 873 K for 2 h, and cooled to room temperature. After the carrier gas was changed to H_2/Ar, the sample was heated to 873 K at a rate of 6 K min^{-1}. Hydrogen consumption was measured by an "online" Varian 3380 gas chromatograph. ICP spectroscopy was also used to detect the actual amount of copper species rudimental in the samples of M5 and aM5.

Instantaneous adsorption of nitrosamines was carried out by the GC method.[56] A 5-mg sample (20–40 mesh) was placed in a stainless-steel microreactor 3 mm in diameter and 150 mm in length, with one end inserted deeply into the injector port and the other end connected to the separation column (10% Carbowax 20 M + 5% KOH, 3 mm diameter, 3000 mm length) of a Varian 3380 gas chromatograph. The reactor was sealed by glass wool to fix the position where the temperature could be accurately controlled by the injector port. The sample was heated directly to the required temperature without activation in carrier gas flowing at a rate of 30 mL min^{-1}, and a solution of nitrosamine (2 μL) was pulse-injected. The thermal-conductivity detector of the gas chromatograph was used to analyze the gaseous effluent, and the decrease in the ratio of solute to solvent was utilized to calculate the adsorbed amount.[43]

To evaluate the reduction efficiency of the cM*n* composites toward nitrosamines in mainstream cigarette smoke, 20-mg samples (20–40 mesh) were carefully added to the filter to replace part of the cellulose matrix with the same volume. Twenty cigarettes were smoked in a glass chamber designed by Miyake and Shibamoto.[57] The rate of airflow was kept at 3 L min^{-1}, and the cigarette smoke was drawn through citrate/phosphate buffer (100 mL) containing ascorbic acid (0.02 mol) to adsorb the nitrosamines. The buffer solution was extracted with dichloromethane, and the combined organic fractions were dried over anhydrous sodium sulfate and concentrated to the final volume of 25 mL. Finally, the mean amount of nitrosamines adsorbed was determined by spectrophotometry.[17]

Acknowledgements

Financial support from the National Science Foundation of China (20673053, 20273031, and 20373024) and the Analysis Center of Nanjing University as well as British American Tobacco (BAT) is gratefully acknowledged.

[1] M. Kruk, M. Jaroniec, S. H. Joo, R. Ryoo, *J. Phys. Chem. B* **2003**, *107*, 2205–2213.
[2] T. D. Tilley, *J. Mol. Catal. A* **2002**, *182–183*, 17–24.
[3] R. Doll, R. Peto, *J. Natl. Cancer Inst.* **1981**, *66*, 1191–1308.
[4] D. M. Parkin, P. Pisani, A. D. Lopez, E. Masuyer, *Int. J. Cancer* **1994**, *59*, 494–504.
[5] *N*-Nitroso compounds: D. H. Fine, D. P. Rounbehler, *ACS Symp. Ser.* **1981**, *174*, 207.
[6] B. Prokopczyk, D. Hoffmann, M. Bologna, A. J. Cunningham, N. Trushin, S. Akerkar, T. Boyiri, S. Amin, D. Desai, S. Colosimo, B. Pittman, G. Leder, M. Ramadani, D. Henne-Bruns, H. G. Beger, K. El-Bayoumy, *Chem. Res. Toxicol.* **2002**, *15*, 677–685.
[7] P. D. Terry, T. E. Rohan, *Cancer Epidemiol. Biomarkers Prev.* **2002**, *11*, 953–971.
[8] E. J. Mitacek, K. D. Brunnemann, D. Hoffmann, T. Limsila, M. Suttajit, N. Martin, L. S. Caplan, *Carcinogenesis* **1999**, *20*, 133–137.
[9] R. Preussmann in *Environmental Carcinogens: Selected Methods of Analysis*, *Vol. 6* (Eds.: R. Preussmann, I. K. O'Neill, G. Eisenbrand, B. Spiegelhalder, H. Bartsch), WHO, IARC, Scientific Publications, Lyon, **1983**, No. 45, p. 3.
[10] S. S. Hecht, *Mutat. Res.* **1999**, *424*, 127–142.
[11] J. R. Williams (Regent Court Technologies), WO 98 05 226, **1997**.
[12] J. M. Lee, J. K. Suh, S. Y. Jeong, H. K. Jin, B. K. Park, C. H. Park, J. H. Park, S. W. Kim (Korea Research Institute of Chemical Technology), WO 97 04 865, **1997**.
[13] D. Hoffmann, M. V. Djordjevic, I. Hoffmann, *Prev. Med.* **1997**, *26*, 427–434.
[14] D. Hoffmann, I. Hoffmann, *J. Toxicol. Environ. Health* **1997**, *50*, 307–364.
[15] M. W. Meier, K. Siegmann, *Microporous Mesoporous Mater.* **1999**, *33*, 307–310.
[16] Y. Wang, B. Shen, J. H. Zhu, L. Ji, L. L. Ma, Q. H. Xu, *Chin. Environ. Chem.* **2000**, *19*, 280–286.

[17] Y. Xu, J. H. Zhu, L. L. Ma, A. Ji, Y. L. Wei, X. Y. Shang, *Microporous Mesoporous Mater.* **2003**, *60*, 125–138.
[18] R. R. Baker in *Tobacco Production, Chemistry and Technology* (Eds.: D. L. Davis, M. T. Nielsen), Blackwell, London, **1999**, p. 419.
[19] J. H. Zhu, S. L. Zhou, Y. Xu, Y. Cao, Y. L. Wei, *Chem. Lett.* **2003**, 338–339.
[20] C. F. Zhou, Y. Cao, T. T. Zhuang, S. L. Zhou, Y. Wang, L. L. Ma, B. Shen, J. H. Zhu, *Stud. Surf. Sci. Catal.* **2005**, *158*, 1003–1011.
[21] F. Martinez, Y.-J. Han, G. D. Stucky, J. L. Sotelo, G. Ovejero, J. A. Melero, *Stud. Surf. Sci. Catal.* **2002**, *142*, 1109–1116.
[22] Y. Xu, Q. Jiang, Y. Cao, Y. L. Wei, Z. Y. Yun, J. H. Xu, Y. Wang, C. F. Zhou, L. Y. Shi, J. H. Zhu, *Adv. Funct. Mater.* **2004**, *14*, 1113–1123.
[23] Y. M. Wang, Z. Y. Wu, Y. L. Wei, J. H. Zhu, *Microporous Mesoporous Mater.* **2005**, *84*, 127–136.
[24] Z. Y. Wu, Y. M. Wang, J. H. Zhu, *Stud. Surf. Sci. Catal.* **2005**, *156*, 139–146.
[25] Y. M. Wang, Z. Y. Wu, L. Y. Shi, J. H. Zhu, *Adv. Mater.* **2005**, *17*, 323–327.
[26] C. F. Zhou, Y. M. Wang, Y. Cao, T. T. Zhuang, W. Huang, Y. Chun, J. H. Zhu, *J. Mater. Chem.* **2006**, *16*, 1520–1528.
[27] M. R. Guerin, R. A. Jenkins, B. A. Tomkins, *Chemistry of Environmental Tobacco Smoke: Composition and Measurement*, Lewis, London, **1992**, p. 90.
[28] Y. M. Wang, Z. Y. Wu, H. J. Wang, J. H. Zhu, *Adv. Funct. Mater.* **2006**, *16*, 2374–2386.
[29] H.-P. Lin, C.-P. Kao, C.-Y. Mou, S.-B. Liu, *J. Phys. Chem. B* **2000**, *104*, 7885–7894.
[30] H.-P. Lin, C.-Y. Mou, *Microporous Mesoporous Mater.* **2002**, *55*, 69–80.
[31] Z. P. Li, L. Gao, *J. Phys. Chem. Solids* **2003**, *64*, 223–228.
[32] S. Velu, L. Wang, M. Okazaki, K. Suzuki, S. Tomura, *Microporous Mesoporous Mater.* **2002**, *54*, 113–126.
[33] J. Patarin, *Angew. Chem.* **2004**, *116*, 3968–3970; *Angew. Chem. Int. Ed.* **2004**, *43*, 3878–3880.
[34] D. P. Serrano, R. van Grieken, J. A. Melero, A. García, *Appl. Catal. A* **2007**, *319*, 171–180.
[35] B. Yuliarto, H. Zhou, T. Yamada, I. Honma, K. Asai, *ChemPhysChem* **2004**, *5*, 261–265.
[36] Z. Konya, J. Zhu, A. Szegedi, I. Kiricsi, P. Alivisatos, G. A. Somorjai, *Chem. Commun.* **2003**, 314–315.
[37] W. Zhang, B. Glomski, T. R. Pauly, T. J. Pinnavaia, *Chem. Commun.* **1999**, 1803–1804.
[38] S. A. Bagshaw, *J. Mater. Chem.* **2001**, *11*, 831–840.
[39] I. Sobczak, M. Ziolek, M. Renn, P. Decyk, I. Nowak, M. Daturi, J.-C. Lavalley, *Microporous Mesoporous Mater.* **2004**, *74*, 23–36.
[40] J. Sarkany, J. L. d'Itri, W. M. H. Sachtler, *Catal. Lett.* **1992**, *16*, 241–249.
[41] C. Göltner-Spickermann, *Curr. Opin. Colloid Interface Sci.* **2002**, *7*, 173–178.
[42] F. L. Slejko, *Adsorption Technology: a Step-by-Step Approach to Process Evaluation and Application*, Marcel Dekker, New York, **1985**.
[43] C. F. Zhou, Y. Cao, T. T. Zhuang, W. Huang, J. H. Zhu, *J. Phys. Chem. C* **2007**, *111*, 4347–4357.
[44] Z.-L. Wang, Q.-S. Liu, J.-F. Yu, T.-H. Wu, G.-J. Wang, *Appl. Catal. A* **2003**, *239*, 87–94.
[45] M. Hartmann, S. Racouchot, C. Bischof, *Microporous Mesoporous Mater.* **1999**, *27*, 309–320.
[46] C. F. Zhou, Y. M. Wang, J. H. Xu, T. T. Zhuang, Y. Wang, Z. Y. Wu, J. H. Zhu, *Stud. Surf. Sci. Catal.* **2005**, *156*, 907–916.
[47] P. Van Der Voort, P. I. Ravikovitch, K. P. De Jong, M. Benjelloun, E. Van Bavel, A. H. Janssen, A. V. Neimark, B. M. Weckhuysen, E. F. Vansant, *J. Phys. Chem. B* **2002**, *106*, 5873–5877.
[48] G. S. Armatas, P. J. Pomonis, *Microporous Mesoporous Mater.* **2004**, *67*, 167–174.
[49] F. Caruso, *Adv. Mater.* **2001**, *13*, 11–22.
[50] C. M. Kowalchuk, G. Schmid, W. Meyer-Zaika, Y. N. Huang, J. F. Corrigan, *Inorg. Chem.* **2004**, *43*, 173–180.
[51] C. T. Kresge, M. E. Leonowicz, W. J. Roth, J. C. Vartuli, J. S. Beck, *Nature* **1992**, *359*, 710–712.
[52] H. Vinh-Thang, Q. Huang, M. Eic, D. Trong-On, S. Kaliaguine, *Langmuir* **2005**, *21*, 2094–2101.
[53] H. Vinh-Thang, Q. Huang, A. Ungureanu, M. Eic, D. Trong-On, S. Kaliaguine, *Langmuir* **2006**, *22*, 4777–4786.
[54] Y. M. Wang, Z. Y. Wu, J. H. Zhu, *J. Solid State Chem.* **2004**, *177*, 3815–3823.
[55] Y. Wang, X. W. Han, A. Ji, L. Y. Shi, S. Hayashi, *Microporous Mesoporous Mater.* **2005**, *77*, 139–145.
[56] Y. Xu, H. D. Liu, J. H. Zhu, Z. Y. Yun, J. H. Xu, Y. L. Wei, *New J. Chem.* **2004**, *28*, 244–252.
[57] T. Miyake, T. Shibamoto, *J. Chromatogr. A* **1995**, *693*, 376–381.

Received: December 9, 2006
Revised: March 15, 2007
Published online: June 19, 2007

